IEEE Access
Multidisciplinary | Rapid Review | Open Access Journal

Received March 9, 2019, accepted March 31, 2019, date of publication April 11, 2019, date of current version April 29, 2019.

Digital Object Identifier 10.1109/ACCESS.2019.2910275

A Fast-Initial Alignment Method With Angular Rate Aiding Based on Robust Kalman Filter

XIANG XU[1], JIAYI LU[1], AND TAO ZHANG[2]
[1]School of Electronic and Information Engineering, Soochow University, Suzhou 215006, China
[2]School of Instrument Science and Engineering, Southeast University, Nanjing 210096, China

Corresponding author: Xiang Xu (hsianghsu@163.com)

This work was supported in part by the Foundation of Key Laboratory of Micro-Inertial Instrument and Advanced Navigation Technology, Ministry of Education, China, under Grant SEU-MIAN-201802, in part by the National Natural Science Foundation of China under Grant 61803278, in part by the National Natural Science Foundation of China under Grant 51375088, in part by the Inertial Technology Key Lab Fund under Grant 614250607011709, in part by the Fundamental Research Funds for the Central Universities under Grant 2242018K40065, in part by the Foundation of Shanghai Key Laboratory of Navigation and Location-Based Services, and in part by the Key Laboratory Fund for Underwater Information and Control under Grant 614221805051809.

ABSTRACT In this paper, a fast-initial alignment method with angular rate aiding based on robust Kalman filter is proposed. First, the traditional system model of the initial alignment is derived, and the angular rate aiding method in the navigation frame is studied. To address the defects of the traditional angular rate aiding alignment method, the angular rate aiding method in body frame is derived. Then, a state augmentation method is employed to address the correlation between process noise and the measurement noise, which exists in the angular rate aiding methods. Considering the practical application, it is hard to keep completely still when the initial alignment is carried out on the vehicle. Therefore, a Huber's M-estimation has been adopted to eliminate the external interferences, and the robustness of the proposed method has been improved. Then, an analytical method for the observability of the proposed method is studied. The reason why the proposed method is faster than the traditional method is analyzed in detail. Finally, simulated and field tests are designed to validate the performance of the proposed method. The results show that the proposed method can finish the initial alignment when it is carried on the vehicle.

INDEX TERMS Strapdown inertial navigation system (SINS), initial alignment, angular rate aiding, robust Kalman filter, state augmentation, analytical observability.

I. INTRODUCTION

Strapdown inertial navigation system (SINS) can provide the real-time attitude, velocity and position of the vehicle with the high output rate [1]. Take the advantage of the SINS, it has been widely applicable in the field of the consumer, industry and military [2]–[5]. Different with the other navigational system, SINS can work in the self-contained state, and the initial attitude, velocity and position is necessary to SINS. Since the initial velocity and position of the vehicle can be easily obtained by the aiding equipment, such as global positioning system (GPS), Doppler velocity log (DVL), long baseline (LBL) transceiver and so on, it is important to acquire the initial attitude of the vehicle for SINS [6]–[8]. The procedure of obtaining the initial attitude for SINS is called initial alignment. And it is the critical step before the SINS works.

The associate editor coordinating the review of this manuscript and approving it for publication was Lubin Chang.

Generally, the initial alignment process can be divided into two categories: one is the coarse alignment process followed by the fine alignment process [9]–[11]; and the other is based on the nonlinear optimal estimation method [12]–[14]. Since the instability of the nonlinear filter method for SINS, the second category has not been widely applicable to the practical system. Thus, many researchers are focus on the first category.

Currently, many methods for the initial alignment process were proposed based on the coarse alignment and the fine alignment process. In [15], [16], an analytical coarse alignment method was investigated, the outputs of the inertial measurement unit (IMU) were used to calculate the initial attitude directly. However, the analytical method cannot finish the coarse alignment in the swaying base, and it is susceptible to the external interferences. Then, the inertial-frame coarse alignment method was proposed to address these defects [17], [18]. Next, the optimization-based attitude

determination method was applicable to the coarse alignment process, the coarse alignment transformed into the continuous attitude determination process [19], [20]. However, the coarse alignment can only provide the initial rough attitude of the SINS, it is limited by the bias of the inertial sensors. Thus, the fine alignment method is often carried out after the coarse alignment to get the more accuracy initial attitude [21]–[26]. Moreover, the fine alignment can estimate the bias of the inertial sensors and velocity and position of the vehicle simultaneously with the attitude estimation. In [21], [22], the observability of the fine alignment was investigated, a method with the piece-wise constant system (PWCS) was used to analyze the observability of the SINS. And then, a multi-position alignment method was investigated to improve the accuracy of the fine alignment method. However, the traditional fine alignment methods take a long time to obtain the acceptable results. Thus, the backtracking methods were studied to improve the convergence rate of the fine alignment methods [24]–[27]. Based on the backtracking methods, the coarse alignment data was reused in the fine alignment process, then the alignment process was prolonging to keep the fine alignment process obtain the limit accuracy.

It is noted that although the coarse and fine alignment is widely used in the practical system, it is hard to set the appropriate parameters for the Kalman filter, which is used in the fine alignment. This defect will cause the fluctuant at the beginning of the fine alignment process. To address this defect, the angular rate, which was the outputs of the gyroscope, was used to faster the convergence rate of the fine alignment methods, and the fluctuation was smoothed [28]–[30]. However, the traditional angular rate aiding methods can only finish the fine alignment method when SINS is under the completely still. If there is any external interference, the alignment process will not get the acceptable results. To address this defect, we proposed a fast-initial alignment method with angular rate aiding based on robust Kalman filter. Based on the robust Kalman filter, the external interferences are eliminated effectively. The advantages of the angular rate aiding method are still going on.

The remainder of this paper is organized as follows. Section II presents the initial alignment with angular rate aiding. The angular rate aiding model in navigational and body frame are studied, respectively. Section III is devoted to the implementation of robust Kalman filter for the angular rate. In Section IV, the observability of the proposed method is analyzed by an analytical algorithm. In Section V, the proposed method and existing alignment methods are compared through the simulation and field tests. Finally, the conclusion is drawn in Section VI.

II. INITIAL ALIGNMENT WITH ANGULAR RATE AIDING

In this section, the initial alignment method with angular rate aiding is derived in detail. Although the system model for SINS is nonlinear with the unknown initial attitude, the linear model is used in this paper, because the initial attitude can be determined fast with the angular rate aiding. Taking the advantage of the angular rate aiding, the large misalignment angles can be determined with the linear error model of SINS, this superiority is also validated by the simulation and field tests.

A. SYSTEM MODEL FOR SINS

In this paper, the alignment process is carried out on the static vehicle. Thus, the system model for initial alignment is based on the Bar-Itzhack-Berman simplified linear SINS error model for small misalignment angles [21], [22]. The state vector used in this paper is given by

$$\boldsymbol{x} = \left[(\boldsymbol{\phi}^n)^T \quad (\delta \boldsymbol{v}^n)^T \quad \left(\boldsymbol{\varepsilon}^b\right)^T \quad \left(\boldsymbol{\nabla}^b\right)^T \right]^T \tag{1}$$

where, $\boldsymbol{\phi}^n = \left[\phi_E^n \ \phi_N^n \ \phi_U^n \right]^T$ denotes the misalignment angle in the navigational frame. $\delta \mathbf{v}^n = \left[\delta v_E^n \ \delta v_N^n \ \delta v_U^n \right]^T$ denotes velocity error in the navigational frame. $\boldsymbol{\varepsilon}^b = \left[\varepsilon_x^b \ \varepsilon_y^b \ \varepsilon_z^b \right]^T$ denotes bias of the gyroscope in the body frame. $\boldsymbol{\nabla}^b = \left[\nabla_x^b \ \nabla_y^b \ \nabla_z^b \right]^T$ denotes bias of the accelerometer in the body frame. It is noted that the superscript n denotes the navigational frame, the corresponding subscript E, N, and U represents the east, north, and up axes in the navigational frame respectively. Similarly, the superscript b denotes the body frame, the corresponding subscript x, y, z and represents the right, forward, and upward axes in the body frame respectively. Then the system equation can be written as

$$\dot{\boldsymbol{x}} = \boldsymbol{F}\boldsymbol{x} + \boldsymbol{\Gamma}\boldsymbol{w} \tag{2}$$

where,

$$\boldsymbol{F} = \begin{bmatrix} \left[\boldsymbol{\omega}_{ie}^n \times\right] & \boldsymbol{R}_c & -\boldsymbol{C}_b^n & \mathbf{0}_{3\times3} \\ \left[\boldsymbol{f}^n \times\right] & -2\left[\boldsymbol{\omega}_{ie}^n \times\right] & \mathbf{0}_{3\times3} & \boldsymbol{C}_b^n \\ \multicolumn{2}{c}{\mathbf{0}_{6\times6}} & \multicolumn{2}{c}{\mathbf{0}_{6\times6}} \end{bmatrix} \tag{3}$$

$$\boldsymbol{R}_c = \begin{bmatrix} 0 & -(R_M + h)^{-1} & 0 \\ (R_N + h)^{-1} & 0 & 0 \\ \tan L\,(R_N + h)^{-1} & 0 & 0 \end{bmatrix} \tag{4}$$

$$\boldsymbol{\Gamma} = \begin{bmatrix} -\boldsymbol{C}_b^n & \mathbf{0}_{3\times3} \\ \mathbf{0}_{3\times3} & \boldsymbol{C}_b^n \\ \multicolumn{2}{c}{\mathbf{0}_{6\times6}} \end{bmatrix} \tag{5}$$

And, $\boldsymbol{w} = \left[\left(\boldsymbol{w}_g^b\right)^{\mathrm{T}} \left(\boldsymbol{w}_a^b\right)^{\mathrm{T}} \right]^{\mathrm{T}}$, where $\boldsymbol{w}_g^b$ and $\boldsymbol{w}_a^b$ represent the measurement noises of the gyroscope and accelerometer. R_N and R_M represent the transverse and meridian radius of the curvature of the WGS-84 reference ellipsoid. L and h are the local latitude and height of the carrier.

The measurement model for the initial alignment on the static base can be given by

$$\boldsymbol{y} = \boldsymbol{H}\boldsymbol{x} + \boldsymbol{\zeta} \tag{6}$$

where, $\boldsymbol{\varsigma}$ represents the measurement noise, and $\boldsymbol{H}$ is given by

$$\boldsymbol{H} = \left[\boldsymbol{I}_{3\times3} \quad \mathbf{0}_{3\times9} \right] \tag{7}$$

It is noted that the measurement $\boldsymbol{y}$ is the velocity errors, which can be given by

$$\boldsymbol{y} = \boldsymbol{v}^n_{SINS} - \tilde{\boldsymbol{v}}^n \tag{8}$$

where, $\boldsymbol{v}^n_{SINS}$ and $\tilde{\boldsymbol{v}}^n$ are, respectively, the output velocity of SINS and the external aiding velocity. When the initial alignment is carried out in the static base, the external aiding velocity can be regarded as the pseudo measurement. Thus, it is a zero vector during the whole alignment process.

The traditional system model of the initial alignment method with state estimation is briefly reviewed in the above statement. However, this system model is based on the small misalignment angle, and a coarse alignment is needed to carry out before the state estimation. Since the initial parameters for the state estimation is correlated with the alignment errors of the coarse alignment method, which are unknown, so the inappropriate initial parameters for state estimation will decrease the performance of the initial alignment with state estimation method, such as the fluctuation at the start of the state estimation and the slow convergence rate of the estimated errors. Considering the static alignment case, the advisable method to address these defects of the traditional methods is augmenting the measurement information with the angular rate [31]. When the alignment ends, the aiding angular rate can be eliminated easily, and the states of the system will not be influenced.

B. ANGULAR RATE MEASUREMENT IN NAVIGATION FRAME

In this subsection, the traditional angular rate measurement model in navigational frame is derived. It is well known that the measurement model of the gyroscope can be modeled as:

$$\tilde{\boldsymbol{\omega}}^b_{ib} = \boldsymbol{\omega}^b_{ib} + \boldsymbol{\varepsilon}^b + \boldsymbol{w}^b_g \tag{9}$$

with,

$$\boldsymbol{\omega}^b_{ib} = \boldsymbol{\omega}^b_{ie} + \boldsymbol{\omega}^b_{en} + \boldsymbol{\omega}^b_{nb} \tag{10}$$

Assuming the carrier keeping completely still, then $\boldsymbol{\omega}^b_{en} = \boldsymbol{\omega}^b_{nb} = \boldsymbol{0}_3$.

When the latitude of the carrier is known, the Earth angular rate in navigational frame can be calculated accurately. Then, the angular rate aiding model can be given by

$$\begin{aligned}\delta\boldsymbol{\omega}^n_{ie} &= \widehat{\boldsymbol{C}}^n_b\tilde{\boldsymbol{\omega}}^b_{ib} - \boldsymbol{\omega}^n_{ie} \\ &= \left(\boldsymbol{I}_{3\times3} - \left[\boldsymbol{\phi}^n\times\right]\right)\boldsymbol{C}^n_b\left(\boldsymbol{\omega}^b_{ie} + \boldsymbol{\varepsilon}^b + \boldsymbol{w}^b_g\right) - \boldsymbol{\omega}^n_{ie} \\ &= \left[\boldsymbol{\omega}^n_{ie}\times\right]\boldsymbol{\phi}^n + \boldsymbol{C}^n_b\boldsymbol{\varepsilon}^b + \boldsymbol{C}^n_b\boldsymbol{w}^b_g - \left[\boldsymbol{\phi}^n\times\right]\boldsymbol{C}^n_b\left(\boldsymbol{\varepsilon}^b + \boldsymbol{w}^b_g\right)\end{aligned} \tag{11}$$

Ignoring the second-order small quantities, (11) can be given by

$$\delta\boldsymbol{\omega}^n_{ie} = \left[\boldsymbol{\omega}^n_{ie}\times\right]\boldsymbol{\phi}^n + \boldsymbol{C}^n_b\boldsymbol{\varepsilon}^b + \boldsymbol{C}^n_b\boldsymbol{w}^b_g \tag{12}$$

In (12), the angular rate aiding model for the traditional method is given. It is noted that the second-order small quantities are ignored. It will decrease the performance of the initial alignment method.

C. ANGULAR RATE MEASUREMENT IN BODY FRAME

In this subsection, an angular rate model in body frame is derived, and the derivation shows that it is more accurate than the traditional method.

Using (9) and (10), it has

$$\begin{aligned}\tilde{\omega}^b_{ib} &= \boldsymbol{\omega}^b_{ie} + \boldsymbol{\varepsilon}^b + \boldsymbol{w}^b_g \\ &= \boldsymbol{C}^b_n\boldsymbol{\omega}^n_{ie} + \boldsymbol{\varepsilon}^b + \boldsymbol{w}^b_g \\ &= \hat{\boldsymbol{C}}^b_n\left(\boldsymbol{I}_{3\times3} - \left[\boldsymbol{\phi}^n\times\right]\right)\boldsymbol{\omega}^n_{ie} + \boldsymbol{\varepsilon}^b + \boldsymbol{w}^b_g \\ &= \hat{\boldsymbol{C}}^b_n\boldsymbol{\omega}^n_{ie} + \hat{\boldsymbol{C}}^b_n\left[\boldsymbol{\omega}^n_{ie}\times\right]\boldsymbol{\phi}^n + \boldsymbol{\varepsilon}^b + \boldsymbol{w}^b_g\end{aligned} \tag{13}$$

Then the angular rate model in the body frame can be given by

$$\begin{aligned}\delta\boldsymbol{\omega}^b_{ie} &= \tilde{\boldsymbol{\omega}}^b_{ib} - \hat{\boldsymbol{C}}^b_n\boldsymbol{\omega}^n_{ie} \\ &= \hat{\boldsymbol{C}}^b_n\left[\boldsymbol{\omega}^n_{ie}\times\right]\boldsymbol{\phi}^n + \boldsymbol{\varepsilon}^b + \boldsymbol{w}^b_g\end{aligned} \tag{14}$$

It is noted that the derivation for (14) does not need to ignore the small quantities. Thus, the accuracy of (14) is better than (12).

In the previous publications, the angular rate $\boldsymbol{\omega}^b_{nb}$ is regarded as the zero vector. However, it is hard to keep zero vector, when alignment process is carried out in the vehicle. Then the augmented model, which shown in (12) and (14), become inaccurate. What's more, the alignment results will also be corrupted by the external interferences.

Considering the external interferences, the angular rate model in body frame can be rewritten as

$$\delta\boldsymbol{\omega}^b_{ie} = \hat{\boldsymbol{C}}^b_n\left[\boldsymbol{\omega}^n_{ie}\times\right]\boldsymbol{\phi}^n + \boldsymbol{\varepsilon}^b + \boldsymbol{\omega}^b_{nb} + \boldsymbol{w}^b_g \tag{15}$$

where, $\boldsymbol{\omega}^b_{nb}$ can be regarded as the external interferences. Inspiring by the robust state estimated principal, the output $\delta\boldsymbol{\omega}^b_{ie}$ can be regarded as the outliers if $\boldsymbol{\omega}^b_{nb}$ is not zero vector. Thus, different with the traditional method, the robust Kalman filter is adopted for this application.

III. ROBUST KALMAN FILTER FOR ANGULAR RATE

In this section, a robust Kalman filter based on the Huber's M-Estimation for angular rate augmented initial alignment is developed. Firstly, the Kalman filter for the initial alignment with the angular rate in body frame is derived. Then, the robust processing is developed.

A. KALMAN FILTER FOR AUGMENTED INITIAL ALIGNMENT

On the basis of the analysis above, we give the discrete filtering model for the angular rate augmented initial alignment straightforwardly

$$\begin{cases}\boldsymbol{x}_k = \boldsymbol{\Phi}_{k,k-1}\boldsymbol{x}_{k-1} + \boldsymbol{G}_{k-1}\boldsymbol{w}_{k-1} \\ \boldsymbol{z}_k = \boldsymbol{\mathcal{H}}_k\boldsymbol{x}_k + \boldsymbol{\eta}_k\end{cases} \tag{16}$$

with

$$\boldsymbol{\Phi}_{k,k-1} = \boldsymbol{I}_{12\times12} + \boldsymbol{F}\Delta t_s \tag{17}$$

$$\boldsymbol{G}_{k-1} = \left(\boldsymbol{I}_{12\times12}+\frac{\boldsymbol{F}\Delta t_s}{2}\right)\boldsymbol{\Gamma}\sqrt{\Delta t_s} \tag{18}$$

$$\boldsymbol{z}_k = \begin{bmatrix} \left(\boldsymbol{y}_k\right)^T & \left(\delta\boldsymbol{\omega}_{ie,k}^b\right)^T \end{bmatrix}^T \tag{19}$$

$$\boldsymbol{\mathcal{H}}_k = \begin{bmatrix} \boldsymbol{0}_{3\times3} & \boldsymbol{I}_{3\times3} & \boldsymbol{0}_{3\times3} & \boldsymbol{0}_{3\times3} \\ \hat{\boldsymbol{C}}_n^b\left[\boldsymbol{\omega}_{ie}^n\times\right] & \boldsymbol{0}_{3\times3} & \boldsymbol{I}_{3\times3} & \boldsymbol{0}_{3\times3} \end{bmatrix} \tag{20}$$

$$\boldsymbol{\eta}_k = \begin{bmatrix} \left(\boldsymbol{\varsigma}_k\right)^T & \left(\boldsymbol{w}_{g,k}^b\right)^T \end{bmatrix}^T \tag{21}$$

It is noted that the augmented measurement noises are correlated with the process noises in (16). Thus, it has

$$E\left[\boldsymbol{w}_k\left(\boldsymbol{\eta}_k\right)^T\right] = \begin{bmatrix} \boldsymbol{0}_{3\times3} & \boldsymbol{Q}_{g,k} \\ \boldsymbol{0}_{3\times3} & \boldsymbol{0}_{3\times3} \end{bmatrix} \tag{22}$$

where, $\boldsymbol{Q}_{g,k} = \mathrm{E}\left[\boldsymbol{w}_{g,k}^b\left(\boldsymbol{w}_{g,k}^b\right)^{\mathrm{T}}\right]$.

There are three categories of methods tuning Kalman filter to address cross-correlation, i.e. de-correlating method, consecutive double predictions and double updates, and state augmentation [31]. In this paper, the augmentation is adopted. Then, the filtering process is given by:

1) PREDICTION

$$\hat{\boldsymbol{x}}_{k,k-1} = \boldsymbol{\Phi}_{k,k-1}\hat{\boldsymbol{x}}_{k-1}+\boldsymbol{G}_{k-1}\begin{bmatrix}\hat{\boldsymbol{w}}_{g,k-1}^b \\ \boldsymbol{0}_3\end{bmatrix} \tag{23}$$

$$\boldsymbol{P}_{k,k-1} = \boldsymbol{\Theta}_{k,k-1}\boldsymbol{\mathcal{P}}_{k-1,k-1}\boldsymbol{\Theta}_{k,k-1}^T+\boldsymbol{G}_{2,k-1}\boldsymbol{Q}_{a,k-1}\boldsymbol{G}_{2,k-1}^T \tag{24}$$

where, $\boldsymbol{Q}_{a,k-1} = \mathrm{E}\left[\boldsymbol{w}_{a,k}^b\left(\boldsymbol{w}_{a,k}^b\right)^T\right]$

$$\boldsymbol{\Theta}_{k,k-1} = \begin{bmatrix}\boldsymbol{\Phi}_{k,k-1} & \boldsymbol{G}_{1,k-1}\end{bmatrix} \tag{25}$$

$$\boldsymbol{\mathcal{P}}_{k-1,k-1} = \begin{bmatrix}\boldsymbol{P}_{k-1,k-1} & \hat{\boldsymbol{P}}_{xg,k-1} \\ \hat{\boldsymbol{P}}_{gx,k-1} & \hat{\boldsymbol{Q}}_{g,k-1}\end{bmatrix} \tag{26}$$

The matrices $\boldsymbol{G}_{1,k-1}$ and $\boldsymbol{G}_{2,k-1}^{\mathrm{T}}$ are the first three columns and the last three columns of the matrix $\boldsymbol{G}_{k-1}$, and $\boldsymbol{G}_{k-1} = \begin{bmatrix}\boldsymbol{G}_{1,k-1} & \boldsymbol{G}_{2,k-1}\end{bmatrix}$.

2) UPDATE

Comprising the augmented state vector and the prior covariance as

$$\hat{\mathbb{X}}_{k,k-1} = \begin{bmatrix}\hat{\boldsymbol{x}}_{k,k-1} \\ \boldsymbol{0}_3\end{bmatrix} \tag{27}$$

$$\boldsymbol{\mathcal{P}}_{k,k-1} = \begin{bmatrix}\boldsymbol{P}_{k,k-1} & \boldsymbol{0}_{12\times3} \\ \boldsymbol{0}_{3\times12} & \boldsymbol{Q}_{g,k-1}\end{bmatrix} \tag{28}$$

Calculating the residual

$$\boldsymbol{e}_k = \boldsymbol{z}_k-\boldsymbol{\mathcal{H}}_k\hat{\boldsymbol{x}}_{k,k-1} \tag{29}$$

Calculating the covariance of the residual

$$\boldsymbol{\mathcal{P}}_e = \boldsymbol{\mathcal{H}}_k\boldsymbol{P}_{k,k-1}\boldsymbol{\mathcal{H}}_k^T-\boldsymbol{R}_k \tag{30}$$

where,

$$\boldsymbol{R}_k = \begin{bmatrix} E\left[\boldsymbol{\varsigma}_k\left(\boldsymbol{\varsigma}_k\right)^T\right] & \boldsymbol{0}_{3\times3} \\ \boldsymbol{0}_{3\times3} & \boldsymbol{Q}_{g,k}\end{bmatrix} \tag{31}$$

Then, the gain matrix is given by

$$\boldsymbol{K}_k = \boldsymbol{\mathcal{P}}_{k,k-1}\begin{bmatrix}\boldsymbol{\mathcal{H}}_k & \boldsymbol{0}_{3\times3} \\ & \boldsymbol{I}_{3\times3}\end{bmatrix}^T\boldsymbol{\mathcal{P}}_e^{-1} \tag{32}$$

The updated state is calculated by

$$\hat{\mathbb{X}}_{k,k} = \begin{bmatrix}\hat{\boldsymbol{x}}_{k,k} \\ \hat{\boldsymbol{w}}_{g,k}^b\end{bmatrix} = \hat{\mathbb{X}}_{k,k-1}+\boldsymbol{K}_k\boldsymbol{e}_k \tag{33}$$

Updating the covariance

$$\boldsymbol{\mathcal{P}}_{k,k} = \begin{bmatrix}\boldsymbol{P}_{k,k} & \hat{\boldsymbol{P}}_{xg,k} \\ \hat{\boldsymbol{P}}_{gx,k} & \hat{\boldsymbol{Q}}_{g,k}\end{bmatrix} = \boldsymbol{\mathcal{P}}_{k,k-1}-\boldsymbol{K}_k\boldsymbol{\mathcal{P}}_e\boldsymbol{K}_k^T \tag{34}$$

Based on the aforementioned steps, the cross correlated Kalman filter with the angular rate aiding method for initial alignment is finished. However, the cross correlated Kalman filter cannot tolerate the interferences of the angular rate $\boldsymbol{\omega}_{nb}^b$. Thus, it is necessary to eliminate these interferences to keep the high accuracy of the initial alignment. One of the effective methods is the robust Kalman filter, and the detailed analysis is given in the next subsection.

B. ROBUST PROCESSING FOR ANGULAR RATE AIDING

In this subsection, the Huber's M-estimation is studied, the angular rate aiding method is regarded as the outlier-contained aiding measurements. Thus, the Huber's M-estimation is defined as the minimization of the following criterion

$$\begin{cases}\hat{\boldsymbol{x}}_{k,k} = \mathrm{argmin}\, J_k\left(\boldsymbol{x}_k\right) \\ J_k\left(\boldsymbol{x}_k\right) = \rho\left(\boldsymbol{\xi}_k\right)\end{cases} \tag{35}$$

where,

$$\xi_k = \left(\sqrt{\boldsymbol{Q}_{g,k}}\right)^{-1}\left(\boldsymbol{z}_{2,k}-\boldsymbol{\mathcal{H}}_{2,k}\boldsymbol{x}_k\right) \tag{36}$$

with

$$\begin{cases}\boldsymbol{z}_{2,k} = \delta\boldsymbol{\omega}_{ie,k}^b \\ \boldsymbol{\mathcal{H}}_{2,k} = \begin{bmatrix}\hat{\boldsymbol{C}}_n^b\left[\boldsymbol{\omega}_{ie}^n\times\right] & \boldsymbol{0}_{3\times3} & \boldsymbol{I}_{3\times3} & \boldsymbol{0}_{3\times3}\end{bmatrix}\end{cases} \tag{37}$$

Choosing the Huber's score function as

$$\rho\left(\boldsymbol{\xi}_k\right) = \begin{cases}\gamma\left|\boldsymbol{\xi}_k\right|-\dfrac{\gamma^2}{2} \\ \dfrac{\xi_k^2}{2}\end{cases} \tag{38}$$

where, γ is chosen to give the desired efficiency at the Gaussian model.

Let $\left.\frac{\partial J_k(\boldsymbol{x}_k)}{\partial \boldsymbol{x}_k}\right|_{\boldsymbol{x}_k=\hat{\boldsymbol{x}}_{k,k}} = \boldsymbol{0}_3$, the weighted function can be solved as

$$\varpi_i = \begin{cases}\gamma\left|\xi_{i,k}\right|-\dfrac{\gamma^2}{2} \\ \dfrac{\xi_{i,k}^2}{2}\end{cases}, \; i = 1,2,3 \tag{39}$$

where, $\xi_{i,k}$ denotes the ith element of $\boldsymbol{\xi}_k$. Considering the influence of the external disturbances, we extend the traditional weighted function as

$$\varpi\left(\xi_{i,k}\right)=\begin{cases}0 & \left|\xi_{i,k}\right|\geq 2\gamma\\ \gamma\left|\xi_{i,k}\right|-\dfrac{\gamma^2}{2} & 2\gamma>\left|\xi_{i,k}\right|\geq\gamma\\ \dfrac{\xi_{i,k}^2}{2} & \left|\xi_{i,k}\right|<\gamma\end{cases},\ i=1,2,3 \tag{40}$$

In (40), it means that when the parameter $\xi_{i,k}$ exceeds more than twice the desired efficiency, it can be regarded as the useless measurement. Then the residual of the real-time filtering process can be calculated as

$$\mathbf{e}_{2,k}=\mathbf{z}_{2,k}-\boldsymbol{\mathcal{H}}_{2,k}\hat{\boldsymbol{x}}_{k,k-1} \tag{41}$$

Define

$$\hat{\xi}_k=\left(\sqrt{\mathbf{Q}}_{g,k}\right)^{-1}\mathbf{e}_{2,k} \tag{42}$$

And the real-time weighted matrix can be given by

$$\mathbb{W}\left(\hat{\xi}_k\right)=\begin{bmatrix}\varpi\left(\hat{\xi}_{1,k}\right) & 0 & 0\\ 0 & \varpi\left(\hat{\xi}_{2,k}\right) & 0\\ 0 & 0 & \varpi\left(\hat{\xi}_{3,k}\right)\end{bmatrix} \tag{43}$$

Then, the robust residual can be calculated by the real-time weighted matrix

$$\hat{\boldsymbol{e}}_{2,k}=\mathbb{W}\left(\hat{\xi}_k\right)\mathbf{e}_{2,k} \tag{44}$$

Lastly, (33) can be rewritten as

$$\hat{\mathbb{X}}_{k,k}=\hat{\mathbb{X}}_{k,k-1}+\mathbf{K}_k\begin{bmatrix}\mathbf{e}_{1,k}\\ \hat{e}_{2,k}\end{bmatrix} \tag{45}$$

Based on the aforementioned steps, the external disturbances can be suppressed by the Huber's M-estimation, and the efficient measurements can be used to update the states.

IV. OBSERVABILITY ANALYSIS

In this section, the observability of the angular rate aiding initial alignment is analyzed by an analytical method. According to the traditional system model (2) and (6), the relationship between the states and the measurements can be given by (46)–(54), [(51), shown at the bottom of this page]

$$\phi_E^n=\frac{\delta\dot{v}_N^n+2\omega_{ie}\sin L\delta v_E^n}{g}-\frac{\nabla_N^n}{g} \tag{46}$$

$$\phi_N^n=-\frac{\delta\dot{v}_E^n-2\omega_{ie}\sin L\delta v_N^n+2\omega_{ie}\cos L\delta v_U^n}{g}+\frac{\nabla_E^n}{g} \tag{47}$$

$$\phi_U^n=\frac{\delta\ddot{v}_N^n+3\omega_{ie}\sin L\delta\dot{v}_E^n-2\left(\omega_{ie}\sin L\right)^2\delta v_N^n}{-g\omega_{ie}\cos L}+\frac{2\omega_{ie}^2\cos L\sin L\delta v_U^n}{-g\omega_{ie}\cos L}+\frac{\nabla_E^n\tan L}{g}-\frac{\varepsilon_E^n}{\omega_{ie}\cos L} \tag{48}$$

$$\varepsilon_E^n=-\frac{\delta\ddot{v}_N^n+2\omega_{ie}\sin L\delta\dot{v}_E^n}{g}+\omega_{ie}\sin L\phi_N^n-\omega_{ie}\cos L\phi_U^n \tag{49}$$

$$\varepsilon_N^n=\frac{\delta\ddot{v}_N^n-2\omega_{ie}\sin L\delta\dot{v}_N^n+2\omega_{ie}\cos L\delta\dot{v}_U^n}{g}-\omega_{ie}\sin L\phi_E^n \tag{50}$$

$$\nabla_E^n=\delta\dot{v}_E^n-2\omega_{ie}\sin L\delta v_N^n+2\omega_{ie}\cos L\delta v_U^n+g\phi_N^n \tag{52}$$

$$\nabla_N^n=\delta\dot{v}_N^n+2\omega_{ie}\sin L\delta v_E^n-g\phi_E^n \tag{53}$$

$$\nabla_U^n=\delta\dot{v}_U^n-2\omega_{ie}\cos L\delta v_E^n \tag{54}$$

It can be easily found that the error ϕ_E^n of pitch is coupling with the equivalent northward bias ∇_N^n of the accelerometer. And, ϕ_N^n is coupling with ∇_E^n. ϕ_U^n is coupling with the ∇_E^n and ε_E^n. These results are compounded with [21], [22]. Thus, there are three unobservable parameters ∇_E^n, ∇_N^n, and ε_E^n. When the multiple position alignment is carried on, the unobservable parameters become observable [23]. Although, the other nine parameters are numerical observable, ϕ_U^n, ε_N^n, and ε_U^n need long alignment time to acquire an acceptable accuracy because they are relating to $\delta\ddot{v}_E^n$, $\delta\ddot{v}_N^n$, and $\delta\ddot{v}_N^n$.

Based on the angular rate aiding model (15), the relationship between states and measurements can be extended as

$$\phi_U^n=\frac{\tilde{z}_E^n}{\omega_{ie}\cos L}-\frac{\delta\dot{v}_E^n-2\omega_{ie}\sin L\delta v_N^n+2\omega_{ie}\cos L\delta v_U^n}{g}\times\tan L+\frac{\nabla_E^n\tan L}{g}-\frac{\varepsilon_E^n}{\omega_{ie}\cos L}-\frac{\tilde{w}_{g,E}^n}{\omega_{ie}\cos L} \tag{55}$$

$$\varepsilon_E^n=\tilde{z}_E^n+\omega_{ie}\sin L\phi_N^n-\omega_{ie}\cos L\phi_U^n-\tilde{w}_{g,E}^n \tag{56}$$

$$\varepsilon_N^n=\tilde{z}_N^n-\omega_{ie}\sin L\phi_E^n-\tilde{w}_{g,N}^n \tag{57}$$

$$\varepsilon_U^n=\tilde{z}_U^n+\omega_{ie}\cos L\phi_E^n-\tilde{w}_{g,U}^n \tag{58}$$

where, $\tilde{z}^n=\begin{bmatrix}\tilde{z}_E^n & \tilde{z}_N^n & \tilde{z}_U^n\end{bmatrix}^T=\hat{C}_b^n\delta\boldsymbol{\omega}_{ie}^b$ and $\tilde{w}_g^n=\begin{bmatrix}\tilde{w}_{g,E}^n & \tilde{w}_{g,N}^n & \tilde{w}_{g,U}^n\end{bmatrix}^T=\hat{C}_b^n\boldsymbol{w}_g^b$.

Comparing (55) and (48), it can be found that the angular rate aiding method faster the convergence rate of ϕ_U^n, because the related term $\delta\ddot{v}_N^n$ is replaced by $\tilde{z}_E^n$. Similarly, the convergence rate of the terms ε_N^n and ε_U^n is improved. However, it is noted that the transformed noises of the gyroscope, which are $\tilde{w}_{g,E}^n$, $\tilde{w}_{g,N}^n$ and $\tilde{w}_{g,U}^n$, will enhance the uncertainty of the estimation. Moreover, the angular rate aiding method will not improve the observability of the initial alignment, because the terms ϕ_E^n, ϕ_N^n, and ϕ_U^n are still coupling with ∇_N^n, ∇_E^n, and ε_E^n, respectively.

Based on the advantage of the angular rate aiding method, the error of yaw will converge rapidly, and it is not limited with the small misalignment condition. Thus, the initial

$$\varepsilon_U^n=\frac{\delta v_N^n+3\omega_{ie}\sin L\delta\ddot{v}_E^n-2\left(\omega_{ie}\sin L\right)^2\delta\dot{v}_N^n+2\omega_{ie}^2\cos L\sin L\delta\dot{v}_U^n}{g\omega_{ie}\cos L}+\omega_{ie}\cos L\phi_E^n \tag{51}$$

alignment can be carried on the arbitrary misalignment angle, and the alignment process need shorter convergence time.

V. PERFORMANCE EVALUATION

A. SIMULATED TEST

In this subsection, a simulation test is designed to validate the performance of the proposed method. Since the engine vibration of the vehicle is hard to simulate, the main purpose of the simulation is focus on the convergence rate and the tolerance for large misalignment angle of the proposed method.

To evaluate the performance of the proposed method, four methods are designed for comparison.

Scheme 1: the traditional OBA coarse alignment method with the pseudo-measurement Kalman filter fine alignment method [20], [22].

Scheme 2: the initial alignment with the angular rate aiding in the navigation frame [30].

Scheme 3: the proposed method with noises-free in the measurements of the IMU, which means the measurements of IMU just contain the bias errors.

Scheme 4: the proposed method with the full noises in the measurement of the IMU.

In the simulated test, a two-position alignment process is designed. For scheme 1, the coarse alignment lasts 50s, and the fine alignment lasts 250s. When the alignment process lasts for 150s, the base rotates 180° to the other position. For other schemes, the initial alignment lasts 300s, and when the initial alignment process lasts for 30s, the base rotates 180° to the other position.

The inertial measurement unit is equipped with a three-axis gyroscope and accelerometer. The bias of the gyroscope is set as $0.02^\circ/h$ and the angular random walk is $0.005^\circ/\sqrt{h}$. The bias of the accelerometer is set as $500\mu g$, and the velocity random walk is $50\mu g/\sqrt{\text{Hz}}$. The sampling interval is set as $\Delta t_s = 0.005$s. The location of the base is set as 32.057313° N (latitude), 118.786365° E (longitude), and 12.34m (height).

The errors of pitch and roll are set as 1°, and the error of yaw is set as 40°. The initial parameters for the proposed method are set as:

$$\begin{aligned}
\mathbf{Q}_{g,k} &= \text{diag}\left(\left[\,8.73\text{e}{-5}\;\; 8.73\text{e}{-5}\;\; 8.73\text{e}{-5}\,\right]^2\right)\\
\mathbf{Q}_{a,k} &= \text{diag}\left(\left[\,4.89\text{e}{-4}\;\; 4.89\text{e}{-4}\;\; 4.89\text{e}{-4}\,\right]^2\right)\\
\mathbf{P}_{0,0} &= \text{diag}\left(\left[\,0.031\;\; 0.031\;\; 48.74\;\; 1e{-4}\;\; 1e{-4}\;\; 1e{-4}\right.\right.\\
&\qquad 2.4\text{e}{-13}\quad 2.4\text{e}{-13}\quad 2.4\text{e}{-13}\\
&\qquad \left.\left.2.4\text{e}{-5}\quad 2.4\text{e}{-5}\quad 2.4\text{e}{-5}\right]\right)\\
\mathbf{R}_k &= \text{diag}\left(\left[\,1\text{e}{-4}\;\; 1\text{e}{-4}\;\; 1\text{e}{-4}\right.\right.\\
&\qquad \left.\left.4.2\text{e}{-10}\;\; 4.2\text{e}{-10}\;\; 4.2\text{e}{-10}\,\right]\right)
\end{aligned}$$

The initial state of the proposed method is set as $\hat{x}_{0,0} = \mathbf{0}_{12}$, $\gamma = 1.5$. Based on the initial parameters, the alignment results are shown in Fig.1 to 5.

In Fig. 1, it is the estimated errors of the bias of the accelerometer. By the two-position alignment process, the bias of the accelerometer is estimated, and the estimated errors of the proposed method are less than $20\mu g$. It is noted that the bias can be estimated by scheme 2 and 4 when the alignment process lasts for 30s. However, the bias estimation of scheme 1 must be finished after the coarse alignment method.

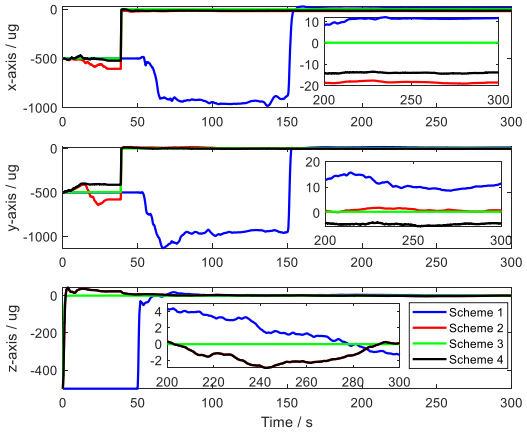

FIGURE 1. The estimated errors of the bias of the accelerometer.

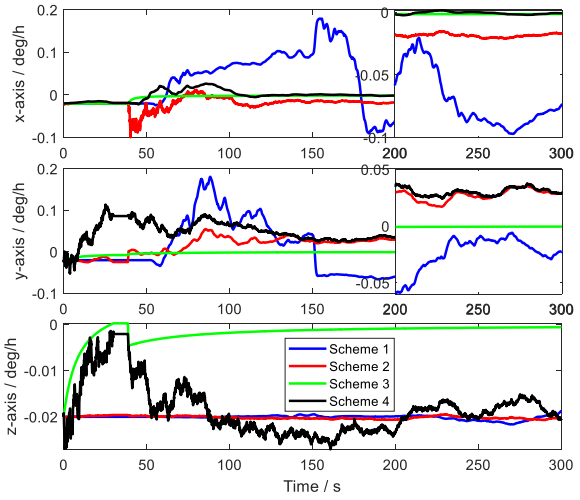

FIGURE 2. The estimated errors of the bias of the gyroscope.

In Fig. 2, the estimated errors of the bias of the gyroscope are shown. It can be found that when there are no measurement noises in the outputs of the IMU, the bias of the gyroscope can be estimated accurately, which is shown as scheme 3. When there are the measurement noises in the outputs of the IMU, the estimated results are fluctuant. Comparing with scheme 1, it can be found that the estimated bias of gyroscope by scheme 2 and 4 is more stable, this is because the alignment process of scheme 2 and 4 can converge to a stable value when it lasts for 300s. The same results can be found in the alignment errors, which are shown in Fig. 3 to 5.

In Fig. 3 and 4, the alignment errors of the pitch and roll are depicted. It can be found that the alignment errors can converge to a stable value rapidly by scheme 2 and 4.

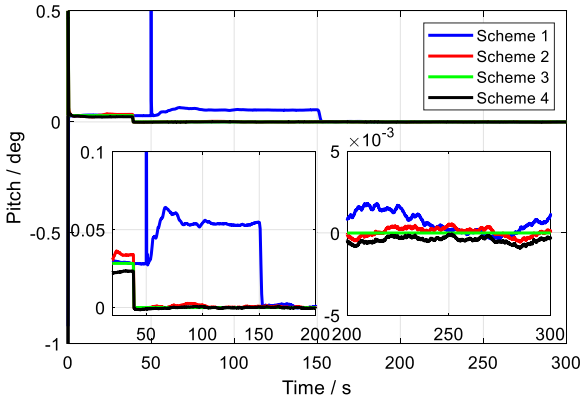

FIGURE 3. The estimated errors of the pitch.

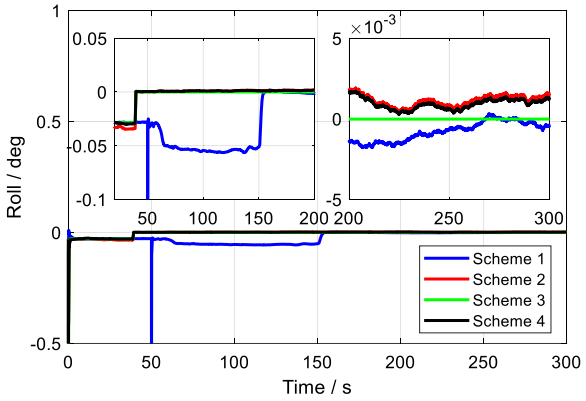

FIGURE 4. The estimated errors of the roll.

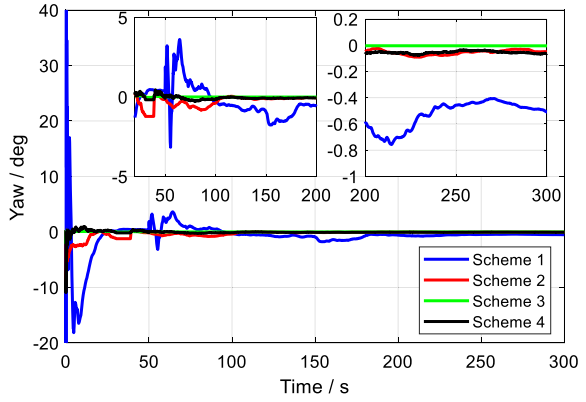

FIGURE 5. The estimated errors of the yaw.

However, the alignment results are fluctuant by scheme 1 from 50s to 150s. This is because, the inappropriate initial parameters are set in the Kalman filter, and the parameters are regulated by the Kalman filter from 50s to 150s. In fact, it is inevitable by scheme 1.

In Fig.5, the alignment results of scheme 2 and 4 converge to the stable value. However, the alignment results of scheme 1 are fluctuant. It is noted that the performance of scheme 2 and 4 is equivalent. This is because the interferences $\boldsymbol{\omega}_{nb}^{b}$ are not contained in the outputs of the gyroscope. However, in the vehicle test, these interferences are contained in the outputs of the gyroscope, then the superiority of scheme 4 will be shown.

B. FIELD TEST

In this subsection, the field test is designed to validate the performance of the proposed method, and the navigational grade inertial measurement unit (IMU), which is equipped with three-axis accelerometer and gyroscope, is used to finish the initial alignment. The sampling rate of the IMU is 200Hz. The specification of the IMU is given in Table 1.

TABLE 1. The specifications of the IMU.

Error item	Gyroscope (x-, y-, z-axes)	Accelerometer (x-, y-, z-axes)
Bias	$\leq (0.05, 0.05, 0.05)$ °/h	$\leq (6, 6, 6)\times 10^{3}$μg
Random walk noise	$\leq (5, 5, 5)\times 10^{-3}$°/$\sqrt{\text{h}}$	$\leq (50, 50, 50)$ μg/$\sqrt{\text{Hz}}$

The whole alignment process lasts 400s. In the first 100s, the vehicle is stationary. Besides, the engine is shut down. From 100s to 175s, the vehicle makes a turn about 170°, and the engine is running until the alignment process is finished. The outputs of the IMU and the true attitude of the vehicle are shown in Fig.6, 7 and 8.

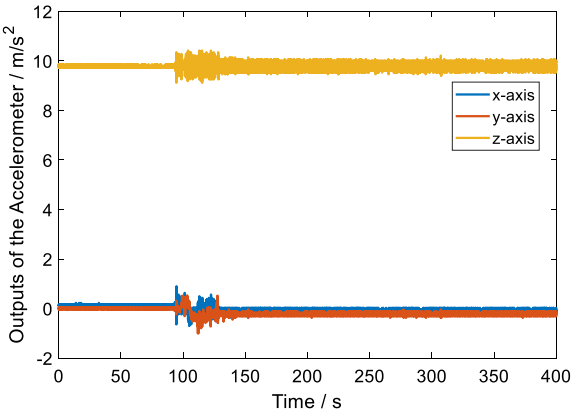

FIGURE 6. The outputs of the accelerometer.

In Fig. 6 and 7, it can be found that the magnitude of the measurement noises of the IMU are different before and after the engine starts. If the angular rate measurement is aided for the initial alignment process, such as the traditional method, the accuracy of the alignment will degrade due to the external interferences. Moreover, when the vehicle makes a turn, the angular rate measurement cannot be used as the aiding information because there are the interferences $\boldsymbol{\omega}_{nb}^{b}$ existing. However, these interferences can be addressed by the proposed method due to the robustness of the proposed method. The initial parameters settings are consistent with the simulation test.

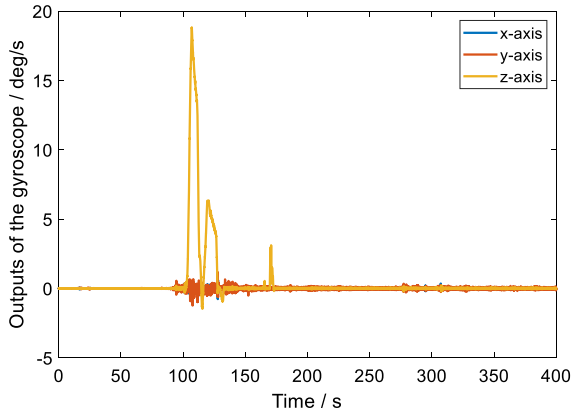

FIGURE 7. The outputs of the gyroscope.

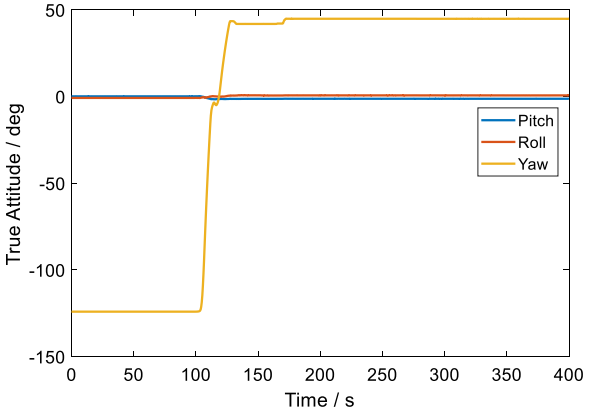

FIGURE 8. The true attitude of the vehicle.

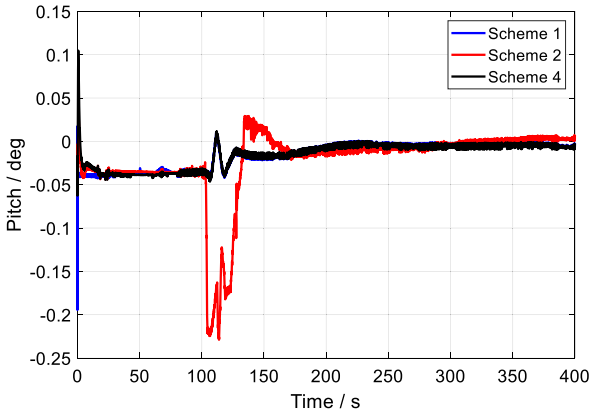

FIGURE 9. The estimated errors of the pitch.

The alignment errors are shown in Fig. 9 to 11. It is noted that the noises of the measurements of the IMU in the practical system cannot be eliminated, thus scheme 3 is removed in the field test.

Since the true bias of the inertial sensors is unknown in the practical system, we remove the bias error figures. In Fig. 9 and 10, the alignment errors of pitch and roll are shown. It can be found that the scheme 1 and 4 have

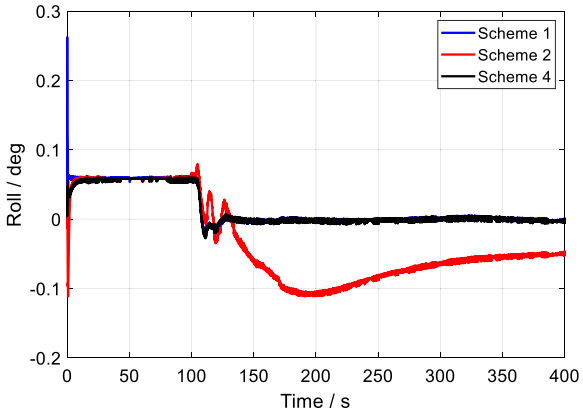

FIGURE 10. The estimated errors of the roll.

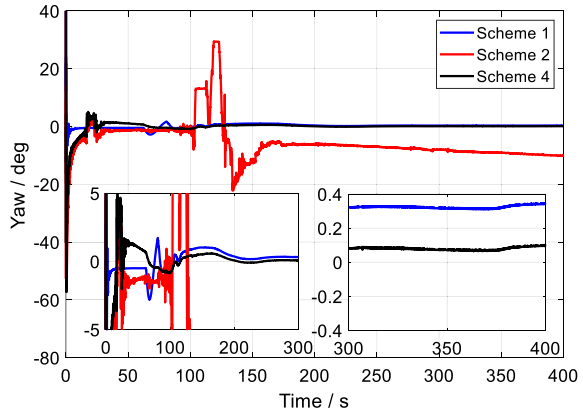

FIGURE 11. The estimated errors of the yaw.

the similar performance. In fact, the turning of the vehicle for scheme 4 can be made earlier. For ease of comparison, the turning of the vehicle is carried out after the coarse alignment. It is noted the alignment results of scheme 2 are failed after 100s due to the external interferences.

In Fig. 11, the yaw errors are shown. It can be clearly found that the alignment errors of scheme 1 are fluctuant after the coarse alignment. Moreover, the alignment errors of scheme 1 are not converging to a stable value, which is larger than 0.3° after 400s. Due to the external interferences, the alignment results of scheme 2 are failed. However, by the advantage of scheme 4, the alignment errors are converging to the stable value rapidly, the alignment error is around 0.1° after 300s.

VI. CONCLUSION

A fast-initial alignment method with angular rate aiding based on robust Kalman filter is proposed in this paper. Firstly, the principal of the initial alignment with the angular rate is studied, and the measurement models with the angular rate in navigation frame and body frame are compared. Then, considering the external interferences, the robust Kalman filter based on Huber's M-estimation is studied. The observability

analysis with an analytical method is studied. By the observability analysis, it can be validated that the convergence rate of the proposed method is faster than the traditional method. Finally, the simulation and field tests are designed to show the performance of the proposed method. The alignment results show that the proposed method is superior to the existing methods. The proposed method can finish the alignment process without the coarse alignment.

VII. ACKNOWLEDGMENT

The authors would like to thank Xiaosu Xu, Tao Zhang, Yao Li, and Yiqing Yao from the School of Instrument Science and Engineering, Southeast University, China, for providing the field tests.

REFERENCES

[1] T. B. Karamat, A. Noureldin, and J. Georgy, *Fundamentals of Inertial Navigation, Satellite-Based Positioning and Their Integration*. Berlin, Germany: Springer, 2013, p. 323.

[2] J. Farrell, *Aided Navigation: GPS With High Rate Sensors*. New York, NY, USA: McGraw-Hill, 2008.

[3] Y. Zhang, C. Shen, J. Tang, and J. Liu, "Hybrid algorithm based on MDF-CKF and RF for GPS/INS system during GPS outages (April 2018)," *IEEE Access*, vol. 6, pp. 35343–35354, 2018.

[4] L. Xu, Z. Xiong, J. Liu, Z. Wang, and Y. Ding, "A novel pedestrian dead reckoning algorithm for multi-mode recognition based on smartphones," *Remote Sens.*, vol. 11, p. 294, Jan. 2019.

[5] Y. Yao, X. Xu, and X. Xu, "An IMM-aided ZUPT methodology for an INS/DVL integrated navigation system," *Sensors*, vol. 17, no. 9, p. 2030, 2017.

[6] T. Zhang, L. Chen, and Y. Yan, "Underwater positioning algorithm based on SINS/LBL integrated system," *IEEE Access*, vol. 6, pp. 7157–7163, 2018.

[7] T. Jinwu, X. Xiaosu, Z. Tao, Z. Liang, and L. Yao, "Study on installation error analysis and calibration of acoustic transceiver array based on SINS/USBL integrated system," *IEEE Access*, vol. 6, pp. 66923–66939, 2018.

[8] Y. Huang and Y. Zhang, "A new process uncertainty robust Student'st based Kalman filter for SINS/GPS integration," *IEEE Access*, vol. 5, pp. 14391–14404, 2017.

[9] X. Xu, X. Xu, T. Zhang, and Z. Wang, "In-motion filter-QUEST alignment for strapdown inertial navigation systems," *IEEE Trans. Instrum. Meas.*, vol. 67, no. 8, pp. 1979–1993, Aug. 2018.

[10] L. Chang, Y. Li, and B. Xue, "Initial alignment for a Doppler velocity log-aided strapdown inertial navigation system with limited information," *IEEE/AMSE Trans. Mechatronics*, vol. 22, no. 1, pp. 329–338, Feb. 2017.

[11] W. Li, W. Wu, J. Wang, and L. Lu, "A fast SINS initial alignment scheme for underwater vehicle applications," *J. Navigat.*, vol. 66, no. 2, pp. 181–198, Mar. 2013.

[12] H. Shao, L. Miao, W. Gao, and J. Shen, "Ensemble particle filter based on KLD and its application to initial alignment of the SINS in large misalignment angles," *IEEE Trans. Ind. Electron.*, vol. 65, no. 11, pp. 8946–8955, Nov. 2018.

[13] J. Li, N. Song, G. Yang, and R. Jiang, "Fuzzy adaptive strong tracking scaled unscented Kalman filter for initial alignment of large misalignment angles," *Rev. Sci. Instrum.*, vol. 87, no. 7, Jul. 2016, Art. no. 075118.

[14] X. Liu, X. Xu, Y. Liu, and L. Wang, "A method for SINS alignment with large initial misalignment angles based on Kalman filter with parameters resetting," *Math. Problems Eng.*, vol. 2014, Apr. 2014, Art. no. 346291.

[15] Y. F. Jiang, "Error analysis of analytic coarse alignment methods," *IEEE Trans. Aerosp. Electron. Syst.*, vol. 34, no. 1, pp. 334–337, Jan. 1998.

[16] N. El-Sheimy, S. Nassar, and A. Noureldin, "Wavelet de-noising for IMU alignment," *IEEE Aerosp. Electron. Syst. Mag.*, vol. 19, no. 10, pp. 32–39, Oct. 2004.

[17] Y. Qin, G. Yan, D. Gu, and J. Zheng, "Clever way of SINS coarse alignment despite rocking ship," *J. Northwestern Polytech. Univ.*, vol. 23, pp. 681–684, Jan. 2005.

[18] W. Sun, A.-G. Xu, and Y. Gao, "Strapdown gyrocompass algorithm for AUV attitude determination using a digital filter," *Measurement*, vol. 46, no. 1, pp. 815–822, 2013.

[19] X. Xu, X. Xu, Y. Yao, and Z. Wang, "In-motion coarse alignment method based on reconstructed observation vectors," *Rev. Sci. Instrum.*, vol. 88, Mar. 2017, Art. no. 035001.

[20] M. Wu, Y. Wu, X. Hu, and D. Hu, "Optimization-based alignment for inertial navigation systems: Theory and algorithm," *Aerosp. Sci. Technol.*, vol. 15, no. 1, pp. 1–17, Jan./Feb. 2011.

[21] I. Y. Bar-Itzhack and B. Porat, "Azimuth observability enhancement during inertial navigation system in-flight alignment," *J. Guid., Control, Dyn.*, vol. 3, pp. 337–344, 1980.

[22] I. Y. Bar-Itzhack and N. Berman, "Control theoretic approach to inertial navigation systems," *J. Guid., Control, Dyn.*, vol. 11, no. 3, pp. 237–245, May 1988.

[23] D. Chung, J. G. Lee, C. G. Park, and H. W. Park, "Strapdown INS error model for multiposition alignment," *IEEE Trans. Aerosp. Electron. Syst.*, vol. 32, no. 4, pp. 1362–1366, Oct. 1996.

[24] H. Xue, X. Guo, Z. Zhou, and K. Wang, "In-motion alignment algorithm for vehicle carried sins based on odometer aiding," *J. Navigat.*, vol. 70, no. 6, pp. 1349–1366, 2017.

[25] W. Li, W. Wu, J. Wang, and M. Wu, "A novel backtracking navigation scheme for autonomous underwater vehicles," *Measurement*, vol. 47, pp. 496–504, Jan. 2014.

[26] T. Du, L. Guo, and J. Yang, "A fast initial alignment for SINS based on disturbance observer and Kalman filter," *Trans. Inst. Meas. Control*, vol. 38, no. 10, pp. 1261–1269, Oct. 2016.

[27] L. Kang, L. Ye, and K. Song, "A fast in-motion alignment algorithm for DVL aided SINS," *Math. Problems Eng.*, vol. 2014, Jun. 2014, Art. no. 593692.

[28] J. C. Fang and D. J. Wan, "A fast initial alignment method for strapdown inertial navigation system on stationary base," *IEEE Trans. Aerosp. Electron. Syst.*, vol. 32, no. 4, pp. 1501–1504, Oct. 1996.

[29] Z. Chuanbin, T. Weifeng, and J. Zhihua, "A novel method improving the alignment accuracy of a strapdown inertial navigation system on a stationary base," *Meas. Sci. Technol.*, vol. 15, no. 4, p. 765, 2004.

[30] G. Chang, "Fast two-position initial alignment for SINS using velocity plus angular rate measurements," *Adv. Space Res.*, vol. 56, pp. 1331–1342, Oct. 2015.

[31] G. Chang, "Alternative formulation of the Kalman filter for correlated process and observation noise," *IET Sci., Meas. Technol.*, vol. 8, pp. 310–318, Apr. 2014.

[32] F. Napolitano, T. Gaiffe, Y. Cottreau, and T. Loret, "PHINS—The first high performances inertial navigation system based on fibre optic gyroscopes," in *Proc. 9th Saint Petersburg Int. Conf. Integr. Navigat. Syst.*, Saint Petersburg, Russia, 2002, pp. 296–304.

XIANG XU was born in Nantong, Jiangsu, in 1988. He received the M.S. degree from Harbin Engineering University, Harbin, China, in 2014, and the Ph.D. degree from Southeast University, Nanjing, China, in 2018.

He is currently a Lecturer with the School of Electronic and Information Engineering, Soochow University. His research interests include initial alignment for inertial navigation, integrated navigation for autonomous underwater vehicle, attitude estimation for low-cost inertial measurement unit, and information fusion.

JIAYI LU was born in Anyang, Henan, in 1998. She is currently pursuing the bachelor's degree with the School of Electronic and Information Engineering, Soochow University.

She is currently studying electronic science and technology. Her research interest includes embedded system development.

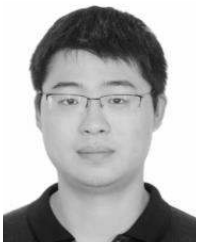

TAO ZHANG received the Ph.D. degree in navigation, guidance, and control from Southeast University, Nanjing, China, in 2008, where he is currently an Associate Professor with the School of Instrument Science and Engineering.

His current research interests include the ship's acoustic navigation systems, long base line, ultra short base line, inertial navigation, integrated navigation, and MEMS inertial technology.